Journal of the Mechanics and Physics of Solids 58 (2010) 1613–1627

Contents lists available at ScienceDirect

Journal of the Mechanics and Physics of Solids

journal homepage: www.elsevier.com/locate/jmps

Continuum theory and phase-field simulation of magnetoelectric effects in multiferroic bismuth ferrite

L.J. Li [a], Y. Yang [a], Y.C. Shu [b], J.Y. Li [a,*]

[a] Department of Mechanical Engineering, University of Washington, Seattle, WA 98195-2600, USA
[b] Institute of Applied Mechanics, National Taiwan University, Taipei 106, Taiwan, ROC

ARTICLE INFO

Article history:
Received 29 April 2010
Received in revised form
25 June 2010
Accepted 5 July 2010

Keywords:
Multiferroics
Bismuth ferrite
Phase field simulation
Antiferromagnetism
Magnetoelectric domain

ABSTRACT

Multiferroic materials possess electric and magnetic orderings simultaneously, making it possible to manipulate the electric state of a multiferroic by magnetic field, or vice versa. Among all single-phase multiferroics, $BiFeO_3$ is particularly exciting, for its room temperature multiferroicity, excellent ferroelectric properties, and recently demonstrated electric control of antiferromagnetic domains, which opens door for its applications in spintronics. In this paper, we report a systematic theoretical and computational study on the structure and evolution of magnetoelectric domains in multiferroic $BiFeO_3$. A continuum description is developed for antiferromagnetic ordering first, which is then incorporated into an unconventional phase field method that couples ferroelastic, ferroelectric, and antiferromagnetic orderings through the characteristic function of variants. The internal elastic, electric, and magnetic fields are carefully analyzed, taking into account both bulk and thin film geometries and boundary conditions. The theory is implemented into numerical simulations, where we not only observe the coupled ferroelectric and antiferromagnetic domains, and demonstrate the electric control of antiferromagnetic ordering, but also reveal the switching of antiferromagnetic domains by mechanical stress that is yet to be reported in experiment. Our study offers deep insight into the microstructural evolution and macroscopic properties of $BiFeO_3$, and provides a powerful tool to study a wide range of multiferroic materials with magnetoelectric coupling.

1. Introduction

Multiferroic materials possess two or more types of orders simultaneously that couple the electric and magnetic fields (Fiebig et al., 2002; Wang et al., 2003; Lottermoser, 2004; Fiebig, 2005; Spaldin and Fiebig, 2005; Nan et al., 2005; Eerenstein et al., 2006; Zhao et al., 2006; Ramesh and Spaldin, 2007; Chu et al., 2008; Balke et al., 2009), rendering them a rich variety of microstructural phenomena and macroscopic properties. For example, it is possible to manipulate the electrical state of a multiferroic material through a magnetic field or vice versa, which is not only appealing scientifically, but also makes the multiferroic materials promising for a wide range of applications (Lottermoser, 2004; Eerenstein et al., 2006; Ramesh and Spaldin, 2007; Chu et al., 2008), including electrically controlled microwave phase shifters or ferromagnetic resonance devices, magnetically controlled electro-optic or piezoelectric devices, broadband magnetic field

---

* Corresponding author. Tel.: +1 206 543 6226; fax: +1 206 685 8047.
E-mail address: jjli@u.washington.edu (J.Y. Li).

0022-5096/$ - see front matter © 2010 Elsevier Ltd. All rights reserved.
doi:10.1016/j.jmps.2010.07.006

sensors, and magnetoelectric memory cells. As a result, there have been renewed interests in magnetoelectric coupling in multiferroic materials, and significant progress has been made in the last few years. For example, the coupled magnetic and electric domains have been observed (Fiebig et al., 2002), and magnetic control of polarization and electric control of magnetization have been demonstrated (Hur et al., 2004; Zhao et al., 2006; Chu et al., 2008; Chung et al., 2009a, b).

Among all multiferroic materials, $BiFeO_3$ is particularly exciting for its rare room temperature multiferroicity, with ferroelectric Curie temperature around 1100 K and antiferromagnetic Neel temperature around 640 K (Kiselev et al., 1963; Teague et al., 1970). It has a rhombohedral crystalline structure, with spontaneous polarization along one of the eight pseudo-cubic [1 1 1] axis, rendering it eight ferroelectric variants (Michel et al., 1969; Kubel and Schimid, 1990; Zavaliche, 2005a, b, 2006; Zhao et al., 2006). Furthermore, it has G-type antiferromagnetic ordering, with magnetic spins perpendicular to [1 1 1] axis, lying in (1 1 1) plane. Within (1 1 1) plane, magnetic spins are ferromagnetically coupled, while between adjacent (1 1 1) planes, they are antiferromagnetically coupled (Zhao et al., 2006; Fischer et al., 1980; Ederer and Spaldin, 2005c). The coupling between the directions of electric polarizations ([1 1 1] axis) and magnetic spins ((1 1 1) plane) makes it possible to control the antiferromagnetic domains of $BiFeO_3$ by electric fields. Indeed, this has been demonstrated in $BiFeO_3$ thin films, where it has been reported that an electric field applied along [0 0 1] axis switches not only the ferroelectric domains, but also antiferromagnetic domains, as observed by a rather sophisticated photoemission electron microscopy (PEEM) based on X-ray linear dichroism (XLD) (Thole et al., 1985; Czekaj et al., 2006; Zhao et al., 2006). By combining this magnetoelectric coupling in antiferromagnetic $BiFeO_3$ with exchange bias in ferromagnetic material, electric control of ferromagnetic ordering has also been demonstrated (Chu et al., 2008), and thus opens door for practical applications of multiferroics in spintronics. This is a very important advance in multiferroics, since antiferromagnetic ordering alone, the most common magnetic ordering in multiferroics, is rather difficult to detect and virtually impossible to use otherwise in applications.

The rapid experimental advances in $BiFeO_3$ are very exciting, but many questions remain to be explored. For example, what is the structure of magnetoelectric domains in $BiFeO_3$, and how does its domain structure evolve under an external stimulus? Answers to these questions are essential to the understanding of the microstructure and macroscopic properties of $BiFeO_3$, and thus are critical to the design, analysis, and application of multiferroic devices based on $BiFeO_3$. While the investigation can be pursued along experimental line, it is rather tedious and expensive, and the sophisticated PEEM and XLD are not easily accessible either. The experimental data from PEEM is sometimes difficult to interpret, and insight from computational modelings will be really helpful. Nevertheless, no computational study on the structure and evolution of magnetoelectric domains in $BiFeO_3$ or any other multiferroics has been reported yet, and only the ferroelectric domain structure of $BiFeO_3$ has been simulated (Cruz et al., 2007; Zhang et al., 2008). The main difficulty lies in the antiferromagnetic domain structure that is challenging to simulate and rarely studied at continuum scale, and the coupling between ferroelectric and antiferromagnetic orderings makes the problem even worse.

Recently, we have developed an unconventional phase field approach that simplifies the computational study of domain structures and their evolution in phase transforming materials substantially (Shu and Yen, 2007). It has been applied successfully to study the twin structure of martensite (Shu and Yen, 2008; Yang and Dayal, 2010) and austenite–martensite interface (Lei et al., 2010), domain structure of ferroelectrics (Shu et al., 2008; Zhang et al., 2010), and coupled magnetoelastic domains in ferromagnetic shape memory alloys (Li et al., 2008a). One of the key advantages of this unconventional phase field method is that it makes the coupling among multiple order parameters much easier to implement, and thus is particularly suitable for studying multiferroics. In this work, we develop a method to simulate the antiferromagnetic domain structure using continuum theory, and combine it with the unconventional phase field approach to study the coupled magnetoelectric domains and cross-field switching in $BiFeO_3$. Compared to first principles calculations that provided deep insight on the quantum mechanical mechanism of multiferrocity (Zhao et al., 2006; Neaton et al., 2005; Ederer and Spaldin, 2005a–c), our continuum study offers fundamental understanding on the microstructures and macroscopic properties of multiferroics that are relevant to materials and devices, and yet are beyond the capability of first principles studies. Some of our preliminary results have been reported in a short letter (Li et al., 2008b), here we systematically present our theory and results in detail.

The paper is organized as follows. A continuum theory is developed for antiferromagnetic coupling of spins in Section 2, and then is incorporated in the energetics of multiferroics with coexistence of ferroelastic, ferroelectric, and antiferromagnetic orderings in Section 3. The kinetics and evolution equations for multiferroic orderings are then developed in Section 4, and the distributions of elastic, electric, and magnetic fields in the multiferroics are solved in Section 5, with two different configurations considered. Finally, detailed numerical simulations and discussions on $BiFeO_3$ are presented in Section 6.

2. Continuum theory of antiferromagnetic coupling

In $BiFeO_3$ lattice, magnetic spins lie in (1 1 1) plane, being ferromagnetically coupled within (1 1 1) plane while antiferromagnetically coupled between adjacent (1 1 1) planes. To develop a continuum description of antiferromagnetic coupling for bismuth ferrite, we consider a lattice of spins $\mathbf{S}^i$, with the short-range exchange interaction between spins given by (Aharoni, 2000; Suess, 2002)

$$W^{af} = -\sum_{i=1}^{N}\sum_{j=1}^{N} J^{ij}\mathbf{S}^i \cdot \mathbf{S}^j, \tag{1}$$

where J^{ij} is the exchange integral whose value depends upon the distance between two spins considered, and N is the total number of spins in the lattice. Notice that for the simplification of notation, we do not explicitly include a factor of $\frac{1}{2}$ in the equation to remove double counting of the pair-wise interactions, but factor it into the exchange integral instead. It is also understood that the spins do not interact with themselves. Due to the short-range nature of exchange coupling, we only consider the exchange interactions between a given spin and its nearest neighbors and the second nearest neighbors. Without loss of generality, we consider a simple cubic lattice, and the relative coordinates of six nearest neighbors with respect to the considered spin are given by (Suess, 2002)

$$\boldsymbol{\delta}^{1,2} = \pm\begin{pmatrix} a \\ 0 \\ 0 \end{pmatrix}, \quad \boldsymbol{\delta}^{3,4} = \pm\begin{pmatrix} 0 \\ a \\ 0 \end{pmatrix}, \quad \boldsymbol{\delta}^{5,6} = \pm\begin{pmatrix} 0 \\ 0 \\ a \end{pmatrix},$$

and those of 12 second-nearest neighbors are given by

$$\zeta^{1,2} = \pm\begin{pmatrix} 0 \\ a \\ -a \end{pmatrix}, \quad \zeta^{3,4} = \pm\begin{pmatrix} a \\ 0 \\ -a \end{pmatrix}, \quad \zeta^{5,6} = \pm\begin{pmatrix} a \\ -a \\ 0 \end{pmatrix},$$

$$\zeta^{7,8} = \pm\begin{pmatrix} 0 \\ a \\ a \end{pmatrix}, \quad \zeta^{9,10} = \pm\begin{pmatrix} a \\ 0 \\ a \end{pmatrix}, \quad \zeta^{11,12} = \pm\begin{pmatrix} a \\ a \\ 0 \end{pmatrix},$$

where a is the lattice constant. Considering only these 18 neighbors, and dividing the lattice of spins into two antiferromagnetically coupled sub-lattices, one with spins $\mathbf{S}^A$, the other with spins $\mathbf{S}^B$, the exchange interaction can be expanded as

$$\begin{aligned} W^{af} &= -\sum_{i=1}^{N/2} J^{ij}\mathbf{S}^A(\mathbf{x}^i)\cdot\sum_{j=1}^{N_b}\mathbf{S}^j - \sum_{m=1}^{N/2} J^{mj}\mathbf{S}^B(\mathbf{x}^m)\cdot\sum_{j=1}^{N_b}\mathbf{S}^j \\ &= -\sum_{i=1}^{N/2} J^{ik}\mathbf{S}^A(\mathbf{x}^i)\cdot\sum_{k=1}^{6}\mathbf{S}^B(\mathbf{x}^i+\boldsymbol{\delta}^k) - \sum_{m=1}^{N/2} J^{mk}\mathbf{S}^B(\mathbf{x}^m)\cdot\sum_{k=1}^{6}\mathbf{S}^A(\mathbf{x}^m+\boldsymbol{\delta}^k) \\ &\quad -\sum_{i=1}^{N/2} J^{in}\mathbf{S}^A(\mathbf{x}^i)\cdot\sum_{n=1}^{12}\mathbf{S}^A(\mathbf{x}^i+\zeta^n) - \sum_{m=1}^{N/2} J^{mn}\mathbf{S}^B(\mathbf{x}^m)\cdot\sum_{n=1}^{12}\mathbf{S}^B(\mathbf{x}^m+\zeta^n), \end{aligned} \tag{2}$$

where $\mathbf{x}^i$ and $\mathbf{x}^m$ are the coordinates of the considered lattice points, and N_b is the number of neighboring points considered. In order to evaluate the summation of the exchange energy, we adopt the following Taylor expansion,

$$\mathbf{S}^{A,B}(\mathbf{x}^i+\boldsymbol{\delta}^k) = \mathbf{S}^{A,B}(\mathbf{x}^i) + \frac{\partial\mathbf{S}^{A,B}(\mathbf{x}^i)}{\partial x_l}\delta_l^k + \frac{1}{2}\frac{\partial^2\mathbf{S}^{A,B}(\mathbf{x}^i)}{\partial x_l\partial x_m}\delta_l^k\delta_m^k,$$

$$\mathbf{S}^{A,B}(\mathbf{x}^i+\zeta^n) = \mathbf{S}^{A,B}(\mathbf{x}^i) + \frac{\partial\mathbf{S}^{A,B}(\mathbf{x}^i)}{\partial x_l}\zeta_l^n + \frac{1}{2}\frac{\partial^2\mathbf{S}^{A,B}(\mathbf{x}^i)}{\partial x_l\partial x_m}\zeta_l^n\zeta_m^n,$$

where the subscripts l and m are used to denote the components of vectors, and repeated subscripts are summed from 1 to 3. Substituting such expansions in Eq. (2), and noticing that due to the symmetry, the summation of the first order terms vanishes over all the considered neighbors, so is the summation of the second order cross product terms, namely $(\partial^2 S^{A,B}/\partial x_l\partial x_m)\zeta_l^n\zeta_m^n$ where $l \neq m$. Furthermore, we denote the exchange integral between the nearest neighbors by J, and that between the second nearest neighbors by $-J'$, indicating their respective antiferromagnetic and ferromagnetic coupling. With these considerations, the short range exchange energy is derived as

$$\begin{aligned} W^{af} &= -12J\sum_{i=1}^{N/2}\mathbf{S}^A(\mathbf{x}^i)\cdot\mathbf{S}^B(\mathbf{x}^i) - Ja^2\sum_{i=1}^{N/2}[\mathbf{S}^A(\mathbf{x}^i)\cdot\Delta\mathbf{S}^B(\mathbf{x}^i) + \mathbf{S}^B(\mathbf{x}^i)\cdot\Delta\mathbf{S}^A(\mathbf{x}^i)] \\ &\quad + 4J'a^2\sum_{i=1}^{N/2}[\mathbf{S}^A(\mathbf{x}^i)\cdot\Delta\mathbf{S}^A(\mathbf{x}^i) + \mathbf{S}^B(\mathbf{x}^i)\cdot\Delta\mathbf{S}^B(\mathbf{x}^i)], \end{aligned} \tag{3}$$

where Δ is the Laplace operator, and a constant $\mathbf{S}(\mathbf{x}^i)\cdot\mathbf{S}(\mathbf{x}^i)$ term is dropped because it is inconsequential to the energetic state of the spin lattice.

Under a continuum approximation, wherein the feature size of the material is much larger than the lattice constant, the distribution of spins $\mathbf{S}^A$ and $\mathbf{S}^B$ can be considered as continuous, and the summation in the exchange energy can be converted to integration. To this end, we introduce magnetic polarization $\mathbf{M}^{a,b}$, the magnetic dipole moment per unit volume, and unit magnetic polarization $\mathbf{m}^{a,b}$ as

$$\mathbf{M}_{a,b}=\frac{\mathbf{S}^{A,B}}{a^3},\quad \mathbf{m}_{a,b}=\frac{\mathbf{M}_{a,b}}{|\mathbf{M}_{a,b}|}=\frac{\mathbf{S}^{A,B}}{s},$$

where s is the magnitude of spin $\mathbf{S}^{A,B}$. As such, the exchange energy can be evaluated as

$$\begin{aligned}W^{af}&=-\frac{12Js^2}{a^3}\sum_{i=1}^{N/2}\mathbf{m}_a(\mathbf{x}^i)\cdot\mathbf{m}_b(\mathbf{x}^i)a^3-\frac{Js^2}{a}\sum_{i=1}^{N/2}[\mathbf{m}_a(\mathbf{x}^i)\cdot\Delta\mathbf{m}_b(\mathbf{x}^i)+\mathbf{m}_b(\mathbf{x}^i)\cdot\Delta\mathbf{m}_a(\mathbf{x}^i)]a^3\\&\quad+\frac{4J's^2}{a}\sum_{i=1}^{N/2}[\mathbf{m}_a(\mathbf{x}^i)\cdot\Delta\mathbf{m}_a(\mathbf{x}^i)+\mathbf{m}_b(\mathbf{x}^i)\cdot\Delta\mathbf{m}_b(\mathbf{x}^i)]a^3\\&=-\frac{6Js^2}{a^3}\int_\square\mathbf{m}_a(\mathbf{x})\cdot\mathbf{m}_b(\mathbf{x})\,dV-\frac{Js^2}{2a}\int_\square[\mathbf{m}_a(\mathbf{x})\cdot\Delta\mathbf{m}_b(\mathbf{x})+\mathbf{m}_b(\mathbf{x})\cdot\Delta\mathbf{m}_a(\mathbf{x})]\,dV\\&\quad+\frac{2J's^2}{a}\int_\square[\mathbf{m}_a(\mathbf{x})\cdot\Delta\mathbf{m}_a(\mathbf{x})+\mathbf{m}_b(\mathbf{x})\cdot\Delta\mathbf{m}_b(\mathbf{x})]\,dV,\end{aligned}$$

where $\square$ is the super-cell of unit volume for continuum evaluation, which is much larger than the unit cell of the lattice. Taking advantages of the divergence theorem and periodic boundary condition, the exchange energy can be simplified as follows:

$$\begin{aligned}W^{af}&=-\frac{6Js^2}{a^3}\int_\square\mathbf{m}_a(\mathbf{x})\cdot\mathbf{m}_b(\mathbf{x})\,dV+\frac{Js^2}{2a}\int_\square[\nabla\mathbf{m}_a(\mathbf{x})\cdot\nabla\mathbf{m}_b(\mathbf{x})+\nabla\mathbf{m}_b(\mathbf{x})\cdot\nabla\mathbf{m}_a(\mathbf{x})]\,dV\\&\quad-\frac{2J's^2}{a}\int_\square[\nabla\mathbf{m}_a(\mathbf{x})\cdot\nabla\mathbf{m}_a(\mathbf{x})+\nabla\mathbf{m}_b(\mathbf{x})\cdot\nabla\mathbf{m}_b(\mathbf{x})]\,dV.\end{aligned}\tag{4}$$

Defining $C=6Js^2/a^3$ and $A_m=-Js^2/2a$, the exchange energy is derived as

$$W^{af}=-\int_\square C\mathbf{m}_a(\mathbf{x})\cdot\mathbf{m}_b(\mathbf{x})\,dV-2A_m\int_\square\nabla\mathbf{m}_a(\mathbf{x})\cdot\nabla\mathbf{m}_b(\mathbf{x})\,dV+A_m\frac{4J'}{J}\int_\square[\nabla\mathbf{m}_a(\mathbf{x})\cdot\nabla\mathbf{m}_a(\mathbf{x})+\nabla\mathbf{m}_b(\mathbf{x})\cdot\nabla\mathbf{m}_b(\mathbf{x})]\,dV.\tag{5}$$

Notice that while the derivation is given for cubic lattice, the continuum expression (5) does not change for different types of lattices, and only the detailed dependence of the continuum constitutive parameters C and A_m on the microscopic parameters such as a and J will be different. If we further assume that the exchange integral $J'=J/4$ for its short-range nature, the exchange energy is finally simplified as

$$W^{af}=\int_\square[A_m|\nabla\mathbf{m}_a(\mathbf{x})-\nabla\mathbf{m}_b(\mathbf{x})|^2-C\mathbf{m}_a(\mathbf{x})\cdot\mathbf{m}_b(\mathbf{x})]\,dV,\tag{6}$$

the expression we will adopt in our following analysis for its simplicity. Notice that the exchange constant A_m is positive while C is negative, so that the first term penalizes the gradient in magnetic polarization, resulting in magnetic domain wall energy, while the second term forces the antiferromagnetic coupling between spins in the two sub-lattices.

3. Energetics of multiferroic state

With a continuum theory of antiferromagnetic coupling established, we now analyze the energetics of multiferroic $BiFeO_3$. In addition to the antiferromagnetic coupling that is represented by the magnetization $\mathbf{m}_a$ and $\mathbf{m}_b$ of two sub-lattices, bismuth ferrite is also ferroelectric with transformation strain $\boldsymbol{\varepsilon}^*$ and spontaneous polarization $\mathbf{p}^*$. As a result, four order parameters are necessary to describe the multiferroic state of bismuth ferrite, which will be discussed in detail next.

3.1. Ferroelectric ordering

We consider the ferroelectric ordering of bismuth ferrite first, which has rhombohedral crystalline structure that is spontaneously polarized along [1 1 1] direction. Due to the reduction in symmetry, a total of eight ferroelectric variants exist, with the transformation strain and spontaneous polarization of each variant given by

$$\boldsymbol{\varepsilon}^{(1,2)}=\begin{pmatrix}\alpha&\delta&\delta\\\delta&\alpha&\delta\\\delta&\delta&\alpha\end{pmatrix},\quad \mathbf{p}^{(1,2)}=\pm\frac{P_s}{\sqrt{3}}\begin{pmatrix}1\\1\\1\end{pmatrix},$$

$$\boldsymbol{\varepsilon}^{(3,4)}=\begin{pmatrix}\alpha&-\delta&-\delta\\-\delta&\alpha&\delta\\-\delta&\delta&\alpha\end{pmatrix},\quad \mathbf{p}^{(3,4)}=\pm\frac{P_s}{\sqrt{3}}\begin{pmatrix}-1\\1\\1\end{pmatrix},$$

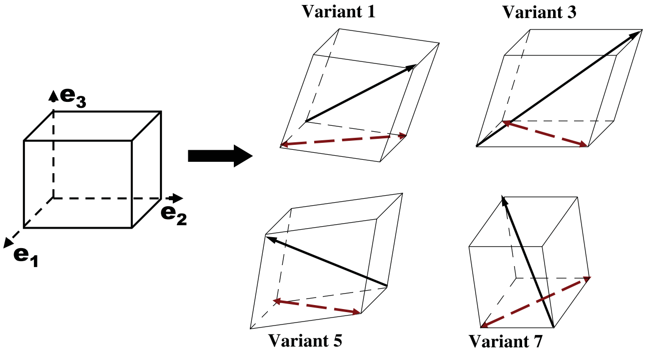

Fig. 1. Schematic of four ferroelastic variants with distinct transformation strain (represented by stretching along one of the body diagonal of the cubic lattice), spontaneous polarization (denoted by solid arrow along the body diagonal), and magnetic easy axis (denoted by dash arrow along the face diagonal that is perpendicular to the body diagonal).

$$\boldsymbol{\varepsilon}^{(5,6)} = \begin{pmatrix} \alpha & -\delta & \delta \\ -\delta & \alpha & -\delta \\ \delta & -\delta & \alpha \end{pmatrix}, \quad \mathbf{p}^{(5,6)} = \pm \frac{P_s}{\sqrt{3}} \begin{pmatrix} 1 \\ -1 \\ 1 \end{pmatrix},$$

$$\boldsymbol{\varepsilon}^{(7,8)} = \begin{pmatrix} \alpha & \delta & -\delta \\ \delta & \alpha & -\delta \\ -\delta & -\delta & \alpha \end{pmatrix}, \quad \mathbf{p}^{(7,8)} = \pm \frac{P_s}{\sqrt{3}} \begin{pmatrix} -1 \\ -1 \\ 1 \end{pmatrix}. \tag{7}$$

These eight ferroelectric variants can be grouped into four ferroelastic variants with distinct transformation strain, as schematically shown in Fig. 1.

In the conventional phenomenological theory of ferroelectrics, polarization is used as the order parameter, and the internal energy density of the ferroelectrics is expanded in terms of the polynomial of polarization (Chen, 2002). This has been very successful in analyzing ferroelectric phase transformation (Hu and Chen, 1998; Li et al., 2002), but involves many material parameters that need to be carefully tuned to yield correct symmetry and energy well structure (Landis, 2008). It is also not easy to couple multiple orderings in the formulation, which becomes increasingly more complicated with the increase of coupled order parameters. As such, this approach is not convenient for simulation of domain structures in multiferroic materials.

To overcome these difficulties, we notice that the transformation strain and spontaneous polarization of the ferroelectric at any particular spatial point can be expressed in terms of the characteristic function of variants and their corresponding transformation strain and spontaneous polarization,

$$\boldsymbol{\varepsilon}^*(\mathbf{x}) = \sum_{i=1}^{8} \lambda_i(\mathbf{x})\boldsymbol{\varepsilon}^{(i)}, \quad \mathbf{p}^*(\mathbf{x}) = \sum_{i=1}^{8} \lambda_i(\mathbf{x})\mathbf{p}^{(i)}, \tag{8}$$

where $\lambda_i(\mathbf{x})$ is the characteristic function of variant i that is specified as

$$\lambda_i(\mathbf{x}) = \begin{cases} 1, & \mathbf{x} \text{ occupied by variant } i, \\ 0 & \text{otherwise}. \end{cases} \tag{9}$$

For rhombohedral bismuth ferrite, there are a total of eight $\lambda_i(\mathbf{x})$ for eight ferroelectric variants, but only seven of them are independent, since they need to satisfy the following constraint:

$$\sum_{i=1}^{8} \lambda_i = 1, \tag{10}$$

so that any spatial point $\mathbf{x}$ is occupied and only occupied by one variant. To incorporate this constraint, we introduce seven independent μ_i that are either 0 or 1, such that

$$\lambda_r = \begin{cases} \mu_r \prod_{i=1}^{r-1}(1-\mu_i), & r = 1, \ldots, 7, \\ \prod_{i=1}^{r-1}(1-\mu_i), & r = 8, \end{cases} \tag{11}$$

which satisfy Eq. (10) automatically. This establishes the equivalence of characteristic functions $\boldsymbol{\mu} = \{\mu_i\}_{i=1}^{7}$ with the transformation strain $\boldsymbol{\varepsilon}^*$ and spontaneous polarization $\mathbf{p}^*$ through Eqs. (8) and (11), allowing us to use them as the internal variables to describe the ferroelectric state instead. The construction (11) is motivated by the multi-rank laminations that are proven energy minimizing for martensitic phase transformation (Bhattacharya, 1993), magnetic materials (DeSimone and James, 2002), and ferroelectrics (Li and Liu, 2004; Tsou and Huber, 2010), and the characteristic function $\boldsymbol{\mu}$ has recently been successfully adopted as the phase field variable to simulate the domain patterns in shape memory alloys (Shu and Yen, 2007, 2008; Yang and Dayal, 2010; Lei et al., 2010), ferroelectric crystals (Shu et al., 2008; Yen et al., 2008; Zhang et al., 2010), and ferromagnetic shape memory alloys (Li et al., 2008a). We adopt the similar strategy here, and propose the following anisotropy ferroelectric energy density,

$$W_{\mu}^{ani}(\boldsymbol{\mu}) = K_{\mu}\sum_{i=1}^{7}\mu_i^2(1-\mu_i)^2, \tag{12}$$

which is minimized by μ_i at either 0 or 1, and thus ensures the multi-well energy structure of bismuth ferrite in the ground state.

When subjected to an external electromechanical loading, both strain $\boldsymbol{\varepsilon}$ and polarization $\mathbf{p}$ might deviate from the ground state, resulting in a piezoelectric energy density as follows:

$$W^{pie}(\boldsymbol{\mu},\mathbf{p}) = \tfrac{1}{2}\,[\boldsymbol{\varepsilon}-\boldsymbol{\varepsilon}^*(\boldsymbol{\mu})]\cdot\mathbf{C}[\boldsymbol{\varepsilon}-\boldsymbol{\varepsilon}^*(\boldsymbol{\mu})]-[\mathbf{p}-\mathbf{p}^*(\boldsymbol{\mu})]\cdot\mathbf{j}[\boldsymbol{\varepsilon}-\boldsymbol{\varepsilon}^*(\boldsymbol{\mu})]+\tfrac{1}{2}[\mathbf{p}-\mathbf{p}^*(\boldsymbol{\mu})]\cdot\boldsymbol{\chi}^{-1}[\mathbf{p}-\mathbf{p}^*(\boldsymbol{\mu})], \tag{13}$$

where the standard quadratic growth away from the energy well is assumed. In the equation, $\mathbf{C}$ is the elastic stiffness, $\mathbf{j}$ is the piezoelectric coefficient, and $\boldsymbol{\chi}$ is the dielectric susceptibility. Notice that strain $\boldsymbol{\varepsilon}$ is not an independent variable in the formulation, and can be determined from the transformation strain $\boldsymbol{\varepsilon}^*$ using mechanical equilibrium equation subjected to differential constraint of compatibility. On the other hand, the polarization is not subjected to such differential constraint. In most ferroelectrics, the induced polarization is much smaller than the spontaneous one, and we can adopt the constrained theory of ferroelectrics (Li and Liu, 2004; Shu et al., 2008), which assumes that the energy-well structure is steep away from the ground state. As such, the polarization $\mathbf{p}$ is restricted within the energy well,

$$\mathbf{p} = \mathbf{p}^*, \tag{14}$$

and the piezoelectric energy density is reduced to the familiar elastic energy density,

$$W^{ela}(\boldsymbol{\mu}) = \tfrac{1}{2}[\boldsymbol{\varepsilon}-\boldsymbol{\varepsilon}^*(\boldsymbol{\mu})]\cdot\mathbf{C}[\boldsymbol{\varepsilon}-\boldsymbol{\varepsilon}^*(\boldsymbol{\mu})]. \tag{15}$$

Through this simplification, the polarization $\mathbf{p}$ is no longer treated as the internal variable, and the ferroelectric state is now completely described by characteristic function $\boldsymbol{\mu}$. It is also noted that within a domain wall, μ_i may deviate from 0 or 1, and thus $\mathbf{p}$ is not necessarily constrained within the energy well across domain walls, as we show later.

3.2. *Antiferromagnetic ordering and magnetoelectric coupling*

As demonstrated in the last section, the energetics of $\mathrm{BiFeO_3}$ is also dependent on magnetization $\mathbf{m}_a$ and $\mathbf{m}_b$ of two sublattices, and excluding the magnetic domain wall energy, the antiferromagnetic energy density is derived from Eq. (6) as

$$W_m^{af}(\mathbf{m}_a,\mathbf{m}_b) = -C\mathbf{m}_a\cdot\mathbf{m}_b, \tag{16}$$

which ensures that $\mathbf{m}_a$ and $\mathbf{m}_b$ are antiferromagnetically coupled. Furthermore, the magnetization prefers to lie in (1 1 1) plane that is perpendicular to [1 1 1], the polar axis of the ferroelectric variant. A uniaxial magnetic anisotropy energy is introduced to reflect this magnetoelectric coupling,

$$W_m^{ani}(\boldsymbol{\mu},\mathbf{m}_{a,b}) = -\frac{K_m}{2}[(\mathbf{m}_a\cdot\mathbf{l}(\boldsymbol{\mu}))^2+(\mathbf{m}_b\cdot\mathbf{l}(\boldsymbol{\mu}))^2], \tag{17}$$

which corresponds to an energy penalty when either $\mathbf{m}_a$ or $\mathbf{m}_b$ rotates away from the magnetic easy axis $\mathbf{l}(\boldsymbol{\mu})$ given by

$$\mathbf{l}(\boldsymbol{\mu}) = \sum_{i=1}^{8}\lambda_i\mathbf{l}^{(i)}. \tag{18}$$

Thus the distribution of magnetic easy axis is given in terms of the characteristic function of variant, with the easy axis of each individual variants given by

$$\mathbf{l}^{(1,2,7,8)} = \begin{pmatrix}1\\ \bar{1}\\ 0\end{pmatrix}, \quad \mathbf{l}^{(3,4,5,6)} = \begin{pmatrix}1\\ 1\\ 0\end{pmatrix}, \tag{19}$$

as established for bismuth ferrite by experimental observations (Zhao et al., 2006) and first principle calculations (Ederer and Spaldin, 2005c). As such, the ferroelectric and antiferromagnetic states are coupled in a straightforward yet physically meaningful manner through the characteristic function $\boldsymbol{\mu}$, without resorting to much more complicated polynomials involving expansions of $\mathbf{p}$, $\boldsymbol{\varepsilon}$, $\mathbf{m}_a$, and $\mathbf{m}_b$.

3.3. Potential energy of multiferroics

We now consider a multiferroic bismuth ferrite occupying a region Ω, and is subjected to an external stress $\boldsymbol{\sigma}^0$, electric field $\mathbf{E}^0$, and magnetic field $\mathbf{H}^0$. The potential energy of the multiferroic is thus given by

$$\begin{aligned}\mathcal{I}(\boldsymbol{\mu},\mathbf{m}_{a,b}) = \int_{\Omega}\{&W^{gra}(\boldsymbol{\mu},\mathbf{m}_{a,b}) + W_{\mu}^{ani}(\boldsymbol{\mu}) + W^{ela}(\boldsymbol{\mu}) + W_{m}^{af}(\mathbf{m}_{a,b}) + W_{m}^{ani}(\boldsymbol{\mu},\mathbf{m}_{a,b})\\ &-\boldsymbol{\sigma}^0\cdot\boldsymbol{\varepsilon} - \mathbf{E}^{\mathbf{0}}\cdot\mathbf{p}^* - M_s\mathbf{H}^{\mathbf{0}}\cdot(\mathbf{m}_a+\mathbf{m}_b)\}\,dV + \frac{\varepsilon_0}{2}\int_{R^3}|\nabla\psi|^2\,dV + \frac{\mu_0}{2}\int_{R^3}|\nabla\phi|^2\,dV,\end{aligned} \tag{20}$$

where

$$W^{gra}(\boldsymbol{\mu},\mathbf{m}_{a,b}) = A_m|\nabla\mathbf{m}_a(\mathbf{x}) - \nabla\mathbf{m}_b(\mathbf{x})|^2 + A_\mu|\nabla\boldsymbol{\mu}|^2 \tag{21}$$

accounts for interfacial energy at domain wall, with the first term describing the magnetic domain wall energy as derived in the last section, and the second term describing the ferroelectric domain wall energy penalizing gradient in $\boldsymbol{\mu}$, and A_μ is the exchange constant for ferroelectric coupling. Notice that works done by the external loadings are subtracted from the total energy. In addition, the last two terms in the potential energy accounts for the depolarization energy and demagnetization energy arising from the interactions among polarizations and magnetizations, with the electric potential ψ and magnetic potential ϕ solved from Maxwell's equations, and ε_0 and μ_0 being the permittivity and permeability of free space.

4. Kinetics

Under an external electric, magnetic or mechanical loading, both $\boldsymbol{\mu}$ and $\mathbf{m}_{a,b}$ will evolve to minimize the potential energy $\mathcal{I}$. The variation of the potential energy $\mathcal{I}$ with respect to $\boldsymbol{\mu}$ and $\mathbf{m}_{a,b}$ is given by

$$\delta\mathcal{I}(\boldsymbol{\mu},\mathbf{m}_{a,b}) = -\int_{\Omega}(\mathbf{F}^{gra} + \mathbf{F}_{\mu}^{ani} + \mathbf{F}^{ela} + \mathbf{F}_{m}^{ani} + \mathbf{F}^{ele})\cdot\delta\boldsymbol{\mu}\,dV - M_s\int_{\Omega}(\mathbf{H}_{a,b}^{gra} + \mathbf{H}_{a,b}^{af} + \mathbf{H}_{a,b}^{ani} + \mathbf{H}^0 - \nabla\phi)\cdot\delta\mathbf{m}_{a,b}\,\mathbf{dV},$$

where periodic boundary conditions have been used in the derivation. The driving forces for the evolution of characteristic function $\boldsymbol{\mu}$ are derived from the energy variation as

$$\mathbf{F}^{gra} = 2A_\mu\nabla^2\boldsymbol{\mu}, \tag{22}$$

$$\mathbf{F}_{\mu}^{ani} = -\frac{\partial}{\partial\boldsymbol{\mu}}W_{\mu}^{ani}(\boldsymbol{\mu}), \tag{23}$$

$$\mathbf{F}^{ela} = \mathbf{C}[\boldsymbol{\varepsilon} - \boldsymbol{\varepsilon}(\boldsymbol{\mu})]\cdot\frac{\partial\boldsymbol{\varepsilon}(\boldsymbol{\mu})}{\partial\boldsymbol{\mu}}, \tag{24}$$

$$\mathbf{F}_{m}^{ani} = -\frac{\partial}{\partial\boldsymbol{\mu}}W_{m}^{ani}(\boldsymbol{\mu},\mathbf{m}_{a,b,}), \tag{25}$$

$$\mathbf{F}^{ele} = (\mathbf{E}^0 - \nabla\psi)\cdot\frac{\partial\mathbf{p}^*}{\partial\boldsymbol{\mu}}, \tag{26}$$

where we have used the following result in deriving the driving force contributed by the depolarization energy:

$$\begin{aligned}\delta\left(\frac{\varepsilon_0}{2}\int_{R^3}|\nabla\psi|^2\,dV\right) &= \varepsilon_0\int_{R^3}\nabla\psi\cdot\nabla(\delta\psi)\,dV = \varepsilon_0\int_{R^3}\nabla\cdot(\psi\nabla(\delta\psi))\,dV - \varepsilon_0\int_{R^3}\psi\nabla^2(\delta\psi)\,dV\\ &= -\int_{R^3}\psi\delta(\varepsilon_0\nabla^2(\psi))\,dV = -\int_{\Omega}\psi\delta(\nabla\cdot\mathbf{p}^*)\,dV\\ &= -\int_{\Omega}\nabla\cdot(\psi\delta\mathbf{p}^*)\,dV + \int_{\Omega}\nabla\psi\cdot\delta\mathbf{p}^*\,dV = \int_{\Omega}\nabla\psi\cdot\delta\mathbf{p}^*\,dV.\end{aligned} \tag{27}$$

On the other hand, the effective fields that drive the evolution of magnetization $\mathbf{m}_{a,b}$ are given by

$$\mathbf{H}_{a,b}^{gra} = \frac{2A_m}{M_s}(\nabla^2\mathbf{m}_{a,b} - \nabla^2\mathbf{m}_{b,a}), \tag{28}$$

$$\mathbf{H}_{a,b}^{af} = \frac{C}{M_s}\mathbf{m}_{b,a}, \tag{29}$$

$$\mathbf{H}_{a,b}^{ani} = -\frac{1}{M_s}\frac{\partial}{\partial\mathbf{m}_{a,b}}W_{m}^{ani}(\boldsymbol{\mu},\mathbf{m}_a,\mathbf{m}_b), \tag{30}$$

where derivation similar to Eq. (27) has been used to derive the contribution from demagnetization energy. Through the driving forces and effective fields, the evolution equations for $\boldsymbol{\mu}$ and $\mathbf{m}_{a,b}$ are established as

$$\frac{\partial \boldsymbol{\mu}}{\partial t} = L[\mathbf{F}^{gra} + \mathbf{F}_{\mu}^{ani} + \mathbf{F}^{ela} + \mathbf{F}_{m}^{ani} + \mathbf{F}^{ele}],$$

$$\frac{\partial \mathbf{m}_{a,b}}{\partial t} = -\gamma_g \mathbf{m}_{a,b} \times \mathbf{H}_{a,b}^{\mathrm{eff}} - \delta\gamma_g \mathbf{m}_{a,b} \times (\mathbf{m}_{a,b} \times \mathbf{H}_{a,b}^{\mathrm{eff}}).$$

The first equation describes a linear kinetic evolution law for $\boldsymbol{\mu}$, with L being the evolution coefficient, while the second equation is in the form of classical Landau–Lifshitz–Gilbert equation (Landau and Lifshitz, 1935; Gilbert, 1955; Brown, 1963; Chen, 2002) that describes the rotation of magnetization $\mathbf{m}_{a,b}$, with the effective magnetic field given by

$$\mathbf{H}_{a,b}^{\mathrm{eff}} = \mathbf{H}_{a,b}^{gra} + \mathbf{H}_{a,b}^{af} + \mathbf{H}_{a,b}^{ani} + \mathbf{H}^{0} - \nabla\phi. \tag{31}$$

5. Elastic, electric, and magnetic fields in the multiferroics

In order to completely determine the energetic state of multiferroics and establish the corresponding driving forces and effective fields for evolution, we need to solve for the strain $\boldsymbol{\varepsilon}$, electric field $\nabla\psi$, and magnetic field $\nabla\phi$ from appropriate governing equations and boundary conditions. To this end, the total strain $\boldsymbol{\varepsilon}$ can be determined by solving mechanical equilibrium equation (Shu et al., 2004; Shu and Yen, 2007, 2008)

$$\nabla \cdot \boldsymbol{\sigma} = \mathbf{0} \text{ in } \Omega, \quad \boldsymbol{\sigma} = \mathbf{C}[\boldsymbol{\varepsilon} - \boldsymbol{\varepsilon}^{*}(\boldsymbol{\mu})], \tag{32}$$

while the electrostatic and magnetostatic fields can be determined by solving Maxwell's equations (Brown, 1963),

$$\nabla \cdot \mathbf{D} = 0 \text{ on } R^3, \quad \mathbf{D} = -\kappa\nabla\psi + \mathbf{p}^{*} \tag{33}$$

and

$$\nabla \cdot \mathbf{B} = 0 \text{ on } R^3, \quad \mathbf{B} = -\mu_0\nabla\phi + \mathbf{m}, \quad \mathbf{m} = \mathbf{m}_a + \mathbf{m}_b. \tag{34}$$

Notice that the dielectric constant $\kappa = \kappa_r\varepsilon_0$ of the multiferroic, instead of the permittivity of the free space ε_0, is used in the dielectric constitutive equation, consistent with the constrained theory of ferroelectric adopted in the last section. Furthermore, the depolarization and demagnetization fields are nonlocal, and could exist in full space, which complicates the analysis. In particular, the electric and magnetic boundary conditions have to be carefully accounted. To this end, we adopt the homogenization theory of ferroelectrics and ferromagnetic materials. Simply put, Maxwell's equations can be decomposed into two parts. One is associated with averaged polarization $\overline{\mathbf{p}}^{*}$ and magnetization $\overline{\mathbf{m}}$ that are uniformly distributed in the domain considered,

$$\nabla \cdot (-\kappa\nabla\overline{\psi} + \overline{\mathbf{p}}^{*}) = 0, \quad \nabla \cdot (-\mu_0\nabla\overline{\phi} + \overline{\mathbf{m}}) = 0. \tag{35}$$

For ellipsoidal domain, the solution are a well known,

$$\nabla\overline{\psi} = \frac{1}{\kappa}\mathbf{N}_{\Omega}\overline{\mathbf{p}}^{*}, \quad \nabla\overline{\phi} = \frac{1}{\mu_0}\mathbf{N}_{\Omega}\overline{\mathbf{m}}, \tag{36}$$

where $\mathbf{N}_{\Omega}$ is the depolarization or demagnetization factor that depends only on the shape aspect ratios of the ellipsoidal domain. The other one is associated with polarization and magnetization fluctuation distributed in a periodic unit cell,

$$\nabla \cdot (-\kappa\nabla\psi' + \mathbf{p}^{*'}) = 0, \quad \nabla \cdot (-\mu_0\nabla\phi' + \mathbf{m}') = 0, \tag{37}$$

which can be solved in Fourier space along with the mechanical equilibrium equation. In the following, two different configurations will be considered, one is two-dimensional bulk material, and the other is thin film. To simplify the notation, the superscript prime will be dropped from all the equations, with the understanding that solutions solved in Fourier space represent field fluctuations.

5.1. Two-dimensional bulk material

The first case we consider is a two-dimensional bulk material, in the sense that all the field variables, such as characteristic functions $\boldsymbol{\mu}$ and magnetization $\mathbf{m}_{a,b}$, are assumed to depend only on x_1 and x_2, so that all terms involving $\partial/\partial x_3$ vanish, even though all the tensorial variables are still three-dimensional in nature. This corresponds to an infinite long cylinder with uniform distribution of field variable along the cylindrical axis, and thus we only need to examine the field distribution in one cross section that is perpendicular to the axis. Implicitly implied in the assumption is that all the interfaces in the material need to be parallel to x_3, and thus only a subset of all possible magnetoelectric domain structures can be captured. Under such configurations, the governing equations can be solved using two-dimensional Fourier transform. In particular, the mechanical displacement field can be solved in Fourier space as (Mura, 1982)

$$\tilde{u}_i(\mathbf{k}) = X_j N_{ij}(\mathbf{k})/D(\mathbf{k}), \tag{38}$$

where

$$X_i = -\mathrm{i}C_{ijkl}\tilde{\varepsilon}^*_{kl}k_j, \tag{39}$$

and $N_{ij}(k)$ and D are cofactors and determinant of the 3×3 matrix $\mathbf{K}$, with

$$K_{ki} = C_{kjil}k_jk_l. \tag{40}$$

Notice that k_i is the coordinates in the two-dimensional Fourier space, and only k_1 and k_2 need to be considered, while all other tensorial variables are three-dimensional. In a similar manner, Maxwell's equation can be solved in two-dimensional Fourier space as

$$\kappa k^2\tilde{\psi} + (k_1\tilde{p}_1^* + k_2\tilde{p}_2^*) = 0 \tag{41}$$

and

$$\mu_0 k^2\tilde{\phi} + (k_1\tilde{m}_1 + k_2\tilde{m}_2) = 0, \tag{42}$$

with $k = \sqrt{k_1^2 + k_2^2}$.

5.2. Two-dimensional thin film

In another extreme, we consider a thin film with thickness much smaller than the in-plane dimension, so that the out-of-plane components of strain can be ignored according to Bhattacharya and James' (1999) theory. As such, all the mechanical tensorial variables are reduced to two-dimensional in nature, and the form of mechanical displacement remains to be the same as Eq. (38), except that all the subscripts can only take 1 and 2 now, and the matrix $\mathbf{K}$ is 2×2 instead of 3×3. The depolarization and demagnetization fields, however, are much more complicated, which we analyze in detail next.

Considering a thin film of thickness h bounded by $0 \le x_3 \le h$, with top and bottom surfaces electroded and periodic boundary condition assumed in x_1–x_2 plane. Then the electric Maxwell's equation and corresponding boundary conditions are given by

$$\nabla\cdot\mathbf{D} = 0, \quad \mathbf{D} = -\kappa\nabla\psi + \mathbf{p}^*, \quad \psi = 0 \text{ at } x_3 = 0,h, \tag{43}$$

which can be transformed into two-dimensional Fourier space as

$$\frac{d^2\tilde{\psi}}{dx_3^2} - k^2\tilde{\psi} = \frac{ik_1\tilde{p_1^*} + ik_2\tilde{p_2^*}}{\kappa} \text{ with } \tilde{\psi}(k_1,k_2,0) = 0, \quad \tilde{\psi}(k_1,k_2,h) = 0. \tag{44}$$

This can be solved in Fourier space as

$$\tilde{\psi} = \frac{c_1}{e^{kh}+1}e^{kx_3} + \frac{c_1e^{kh}}{e^{kh}+1}e^{-kx_3} - c_1, \quad c_1 = \frac{ik_1\tilde{p_1^*} + ik_2\tilde{p_2^*}}{\kappa k^2}. \tag{45}$$

Therefore, the depolarization field $\mathbf{E}^d$ in Fourier space can be derived as

$$\tilde{E_1^d} = \frac{-ik_1}{h}\int_0^h \tilde{\psi}\,dx_3 = -ik_1c_1\left(\frac{2}{kh}\tanh\left[\frac{kh}{2}\right] - 1\right),$$

$$\tilde{E_2^d} = \frac{-ik_2}{h}\int_0^h \tilde{\psi}\,dx_3 = -ik_2c_1\left(\frac{2}{kh}\tanh\left[\frac{kh}{2}\right] - 1\right),$$

$$\tilde{E_3^d} = \frac{1}{h}\int_0^h -\frac{d\tilde{\psi}}{dx_3}dx_3 = 0, \tag{46}$$

which are averaged over the film thickness.

The demagnetization can be solved in a similar manner. However, due to the lack of magnetic monopoles screening at the top and bottom surfaces, the boundary condition is much more complicated, and Maxwell's equation has to be solved in full space. In particular, three regimes have to be considered in the two-dimensional Fourier space,

$$\frac{d^2\tilde{\phi}}{dx_3^2} - (k_1^2 + k_2^2)\tilde{\phi} = 0, \quad x_3 > h,$$

$$\frac{d^2\tilde{\phi}}{dx_3^2} - (k_1^2 + k_2^2)\tilde{\phi} = \frac{ik_1\tilde{m}_1 + ik_2\tilde{m}_2}{\mu_0}, \quad 0 \le x_3 \le h,$$

$$\frac{d^2\tilde{\phi}}{dx_3^2} - (k_1^2 + k_2^2)\tilde{\phi} = 0, \quad x_3 < 0. \tag{47}$$

Taking boundary conditions at infinity into account, the solutions can be derived as follows:

$$\tilde{\phi} = \frac{e^{kh}-1}{2k}\left(\frac{\tilde{m}_3}{\mu_0}-kc_2\right)e^{-kx_3}, \quad h<x_3,$$

$$\tilde{\phi} = \frac{e^{-kh}}{2k}\left(\frac{\tilde{m}_3}{\mu_0}+kc_2\right)e^{kx_3}-\frac{1}{2k}\left(\frac{\tilde{m}_3}{\mu_0}-kc_2\right)e^{-kx_3}-c_2, \quad 0\le x_3\le h,$$

$$\tilde{\phi} = \frac{e^{-kh}-1}{2k}\left(\frac{\tilde{m}_3}{\mu_0}+kc_2\right)e^{kx_3}, \quad x_3<0, \tag{48}$$

with

$$c_2 = \frac{ik_1\tilde{m}_1+ik_2\tilde{m}_2}{\mu_0 k^2}.$$

The demagnetization field in Fourier space can then be derived as

$$\tilde{H}_1^d = \frac{-ik_1}{h}\int_0^h \tilde{\phi}\, dx_3 = ik_1c_2\left(\frac{e^{-kh}+kh-1}{kh}\right),$$

$$\tilde{H}_2^d = \frac{-ik_2}{h}\int_0^h \tilde{\phi}\, dx_3 = ik_2c_2\left(\frac{e^{-kh}+kh-1}{kh}\right),$$

$$\tilde{H}_3^d = \frac{1}{h}\int_0^h -\frac{d\tilde{\phi}}{dx_3}dx_3 = \left(\frac{e^{-kh}-1}{kh}\right)\frac{\tilde{m}_3}{\mu_0}, \tag{49}$$

which are also averaged over the film thickness. These solutions also apply to the depolarization field if the top and bottom surfaces of the film is not electroded, and thus unscreened by charges, if we replace μ_0 by κ, and $\mathbf{m}$ by $\mathbf{p}^*$.

6. Results and discussions

The theory has been implemented into numerical simulation to investigate the magnetoelectric domains and cross-field switching in bulk bismuth ferrite crystal and thin film, with the evolution equations solved by semi-implicit finite difference method on time scale and fast Fourier transform on spatial scale (Chen, 2002; Zhang and Chen, 2005). In this section, we present these results in detail.

6.1. Two-dimensional bulk crystal

We first examine the magnetoelectric domains in bulk bismuth ferrite crystal, with the material parameters (Wang et al., 2003; Ruette et al., 2004; Eerenstein et al., 2005; Zhang et al., 2007) used in the simulation listed in Table 1. The ferroelastic, ferroelectric, and antiferromagnetic domain structures of a clamped bismuth ferrite crystal in the absence of external fields are shown in the top row of Fig. 2, and it is observed that four ferroelastic variants are arranged in a characteristic rank-2 laminate structure, which is further divided into eight ferroelectric domains in a self-accommodating and compatible manner. The arrows in Fig. 2b indicate the directions of in-plane polarization components, while the directions of out-of-plane polarization component are indicated by + and − signs. Only two antiferromagnetic variants are observed, with their spins oriented along [1 1 0] and [1 $\bar{1}$ 0], as indicated by the yellow arrow in Fig. 2c. The direction of sublattice spin $\mathbf{m}_a$ is shown, while the sublattice spin $\mathbf{m}_b$ is antiparallel to $\mathbf{m}_a$. In the bottom row of Fig. 2, the variations of $\boldsymbol{\mu}$, $\mathbf{p}$, and $\mathbf{m}$ on the upper boundary of domains are shown, and clearly the characteristic functions $\boldsymbol{\mu}$ across domain walls deviate from 0 or 1, resulting in reduction in the magnitude of spontaneous polarizations within the domain walls, as we mentioned earlier and consistent with conventional phenomenological theory. On the other hand, while components of magnetization do vary across domain walls, the magnitude of magnetization remains to be constant, as expected from magnetization rotation. These suggest that the structure of domain walls emerging from our simulations is not much different from the conventional theory.

It is noted that ferroelectric variants separated by 180° [variants (1)/(2), (3)/(4), (5)/(6), (7)/(8)] or 109° [variants (1)/(8), (2)/(7), (3)/(6), and (4)/(5)] domain walls share the same antiferromagnetic ordering, while variants (1)/(4) and (6)/(7) are separated by 71° domain wall that also changes the antiferromagnetic ordering, suggesting the possibility of electric

Table 1
Material parameters of bulk bismuth ferrite crystal.

C_{11} (GPa)	C_{12} (GPa)	C_{44} (GPa)	P_s (C/m^2)	M_s (T)	K_m (J/m^3)	K_μ (J/m^3)	κ_r
302	162	68	0.061	0.19	6.6×10^4	6.6×10^5	70

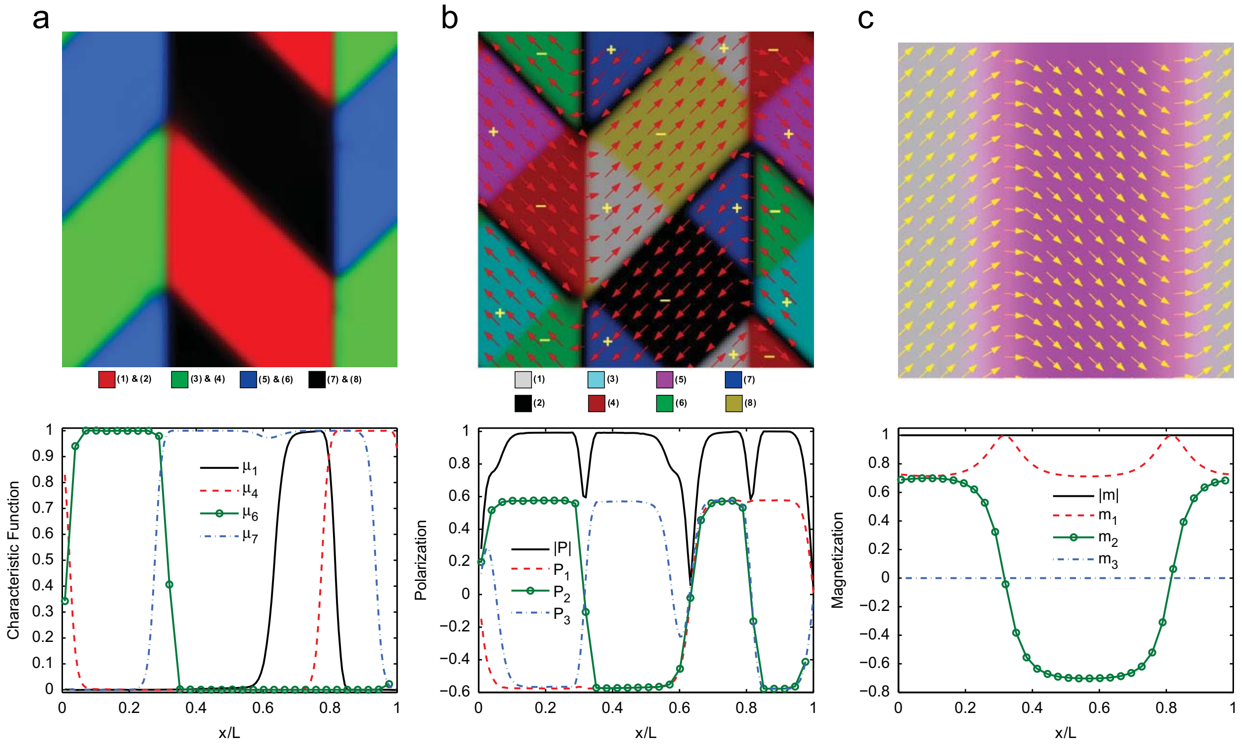

Fig. 2. (a) Ferroelastic, (b) ferroelectric, and (c) antiferromagnetic domains in bulk bismuth ferrite in the absence of applied fields; the top row shows the domain patterns, while the bottom row shows the corresponding variations of $\boldsymbol{\mu}$, $\mathbf{p}$ and $\mathbf{m}$ on the upper boundary of domains; the depolarization factors induced by shape effect is diag$[\frac{1}{3},\frac{1}{3},\frac{1}{3}]$.

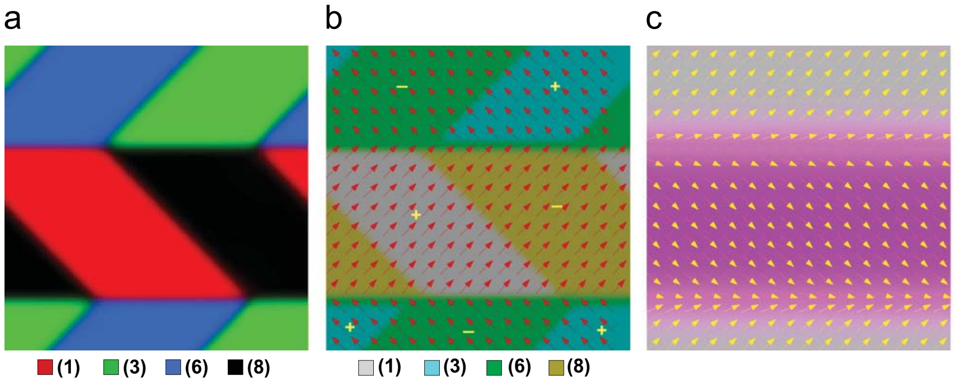

Fig. 3. (a) Ferroelastic, (b) ferroelectric, and (c) antiferromagnetic domains in bulk bismuth ferrite under an in-plane electric field E_2, evolved from the configuration shown in Fig. 2; only four ferroelectric variants (1), (3), (6) and (8) with polarization p_2 along x_2 coexist, and the depolarization factor is diag$[\frac{1}{3},\frac{1}{3},\frac{1}{3}]$.

control of antiferromagnetic ordering through the corresponding 109° ferroelectric domain switching, as observed in experiments (Zhao et al., 2006; Chu et al., 2008). To verify this, an in-plane electric field is applied along x_2-axis to the crystal with the initial domain configuration shown in Fig. 2, and the resulting ferroelastic, ferroelectric, and antiferromagnetic domains are shown in Fig. 3. As expected, the applied electric field eliminates four of the ferroelectric variants, (2), (4), (5), and (7), and the remaining variants (1), (3), (6), and (8) all have polarization p_2 aligned along the applied electric field, as shown in Fig. 3b. What is interesting is that while the electric field effectively eliminates 180° domain wall, the evolution path from Figs. 2b to 3b appears rather complex and non-intuitive. Instead of simply moving the 180° domain walls, all three types of ferroelectric domain walls are moved. As a result of such complex evolution, the final ferroelastic domain pattern in Fig. 3a appears to be 90° rotation from the original one shown in Fig. 2a, so does the antiferromagnetic domain shown in Fig. 3c. Nevertheless, the antiferromagnetic domains are indeed switched by the applied electric field, confirming the magnetoelectric coupling in bismuth ferrite crystal. Similar evolution process is

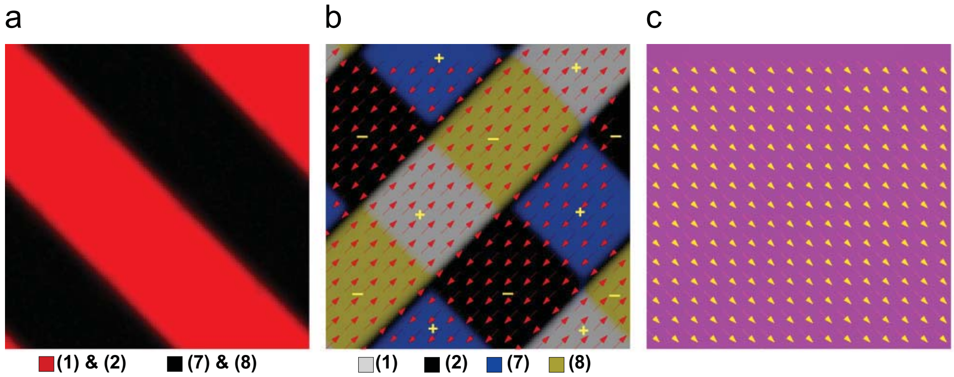

Fig. 4. (a) Ferroelastic, (b) ferroelectric, and (c) antiferromagnetic domains in bulk bismuth ferrite under a shear stress σ_{12}, evolved from the configuration shown in Fig. 2. In this case, four ferroelectric variants (1), (2), (7) and (8) preferred by the shear stress coexist, and the depolarization factor is diag[$\frac{1}{3}$,$\frac{1}{3}$,$\frac{1}{3}$].

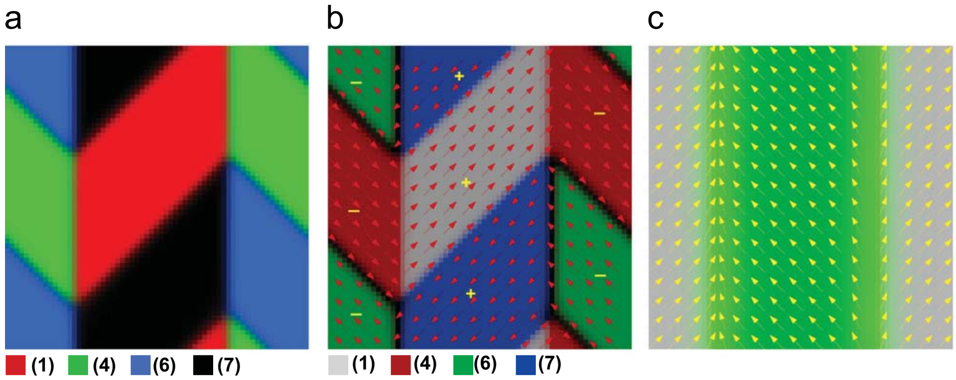

Fig. 5. (a) Ferroelastic, (b) ferroelectric, and (c) antiferromagnetic domains in bismuth ferrite thin film in the absence of applied fields, with four ferroelectric variants (1), (4), (6) and (7) coexisting. The depolarization factor used is diag[0.07,0.07,0].

Table 2
Material parameters of bismuth ferrite thin film.

C^f_{11} (Gpa)	C^f_{12} (Gpa)	C^f_{44} (Gpa)	P_s (C/m^2)	M_s (T)	K_m (J/m^3)	K_μ (J/m^3)	κ_r
215.1	75.1	68	0.91	0.19	6.6×10^4	3.3×10^6	70

also observed when an in-plane electric field is applied along x_1-axis after the crystal field is subjected to a field along x_2, and we are currently investigating the detailed evolution paths and their implications on magnetoelectric response of bismuth ferrite.

Since the ferroelectric and antiferromagnetic domains in bismuth ferrite are effectively coupled through the lattice structure, it is also expected that the antiferromagnetic domains can be switched by an applied mechanical stress. To verify this, a shear stress σ_{12} is applied to the crystal in the absence of an electric field, with the initial domain configuration given by Fig. 2. The resulting ferroelastic, ferroelectric, and antiferromagnetic domains are shown in Fig. 4, and indeed a uniform spin distribution emerges, suggesting that the antiferromagnetic domains are switched by the applied stress. Two of the ferroelastic variants disfavored by the shear stress are eliminated, resulting in a simple rank-one twin structure in ferroelastic domains. Each of the ferroelastic variant is further divided into two ferroelectric variants separated by 180° domain walls, and the resulting ferroelectric domain pattern appears to be check-board type. Such mechanical manipulation of antiferromagnetic domains has yet to be reported in experiments, and we believe it offers additional control over the magnetoelectric coupling that could be useful in a range of applications.

6.2. *Two-dimensional thin films*

We then examine the magnetoelectric domains in bismuth ferrite thin film in the absence of electric field, as shown in Fig. 5 for its ferroelastic, ferroelectric, and antiferromagnetic domains. The material parameters (Wang et al., 2003; Ruette et al., 2004; Eerenstein et al., 2005; Zhang et al., 2007) used in the simulation are listed in Table 2. While both ferroelastic and antiferromagnetic domains appear to be similar to those observed in bulk bismuth ferrite in the absence of electric

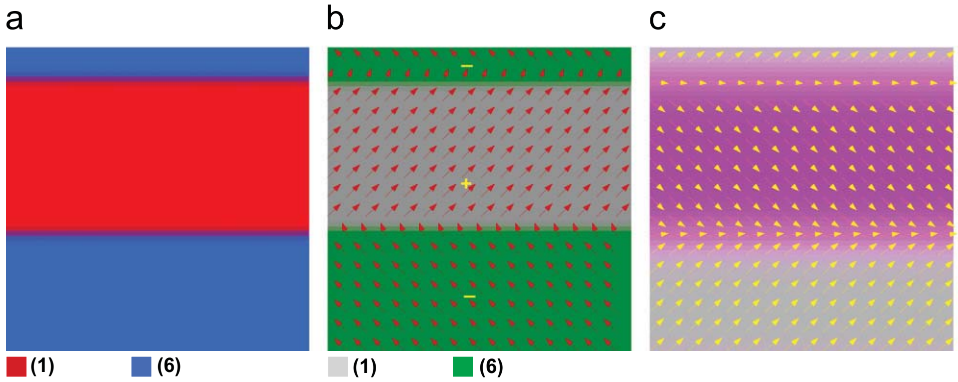

Fig. 6. (a) Ferroelastic, (b) ferroelectric, and (c) antiferromagnetic domains in bismuth ferrite thin film under an in-plane electric field E_2, evolved from the configuration shown in Fig. 5. In this case, only two ferroelectric variants (1) and (6) preferred by the electric field coexist, and the depolarization factor used is diag[0.07,0.07,0].

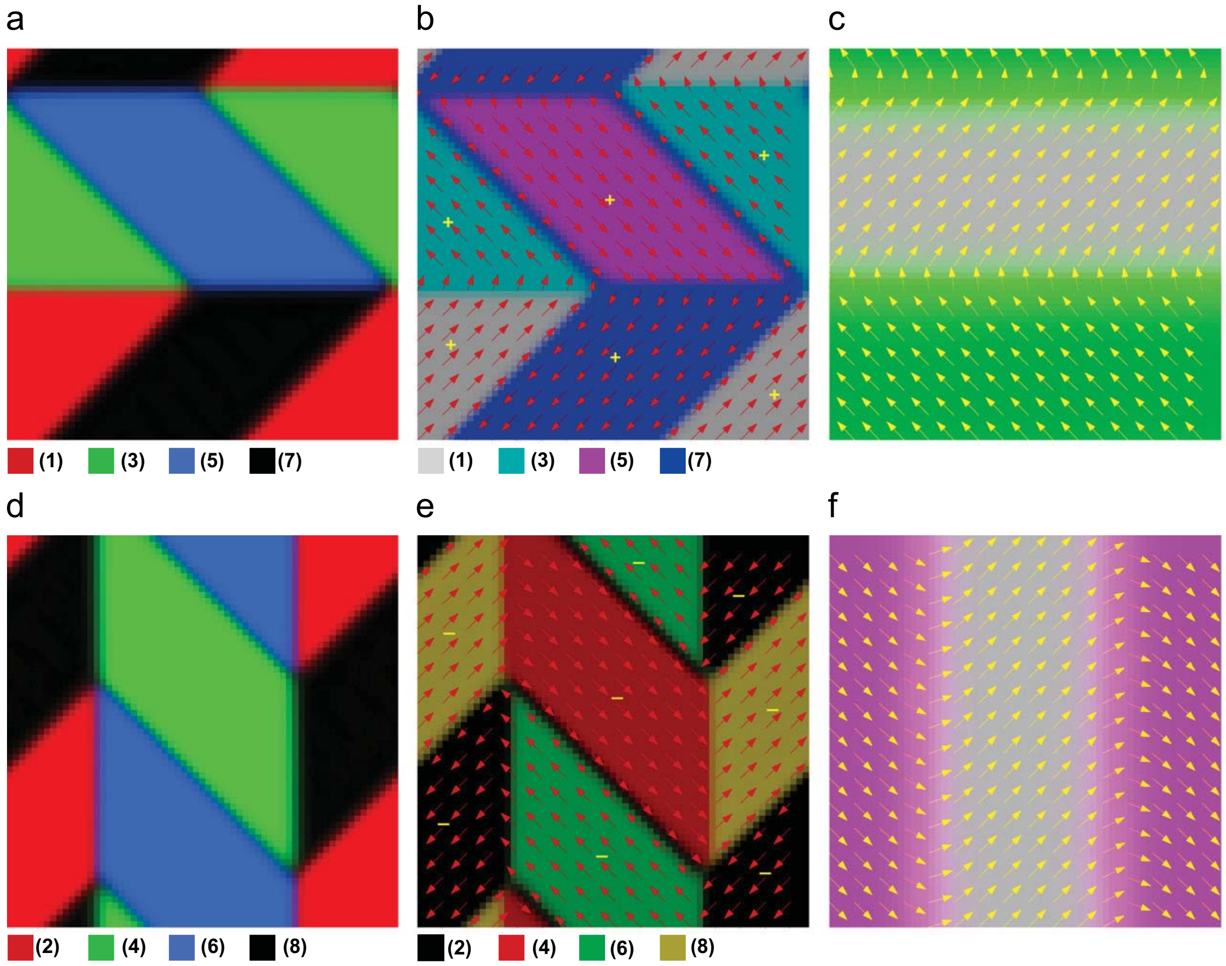

Fig. 7. (a,d) Ferroelastic, (b,e) ferroelectric, and (c,f) antiferromagnetic domains in bismuth thin film under a positive (upper row) and negative (lower row) out-of-plane electric field. The depolarization factor used is diag[0.07,0.07,0].

field, the ferroelectric domains appear to be distinctly different. Only four ferroelectric variants (1), (4), (6) and (7) are observed coexisting, instead of all eight ferroelectric variants observed in bulk bismuth ferrite, because of charge screening at the top and bottom surfaces. Nevertheless, the coupling between ferroelastic, ferroelectric, and antiferromagnetic domains are evident, suggesting the possibility of either electric or mechanical switching of antiferromagnetic domains in bismuth ferrite thin film. For example, under an in-plane electric field E_2, two of the ferroelectric variants (4) and (7) disfavored by the applied electric field disappear, leaving variants (1) and (6) forming a rank-1 laminated domain structure in the thin film, as shown in Fig. 6. Associated with this ferroelectric switching, both ferroelastic and antiferromagnetic domains are also switched by the applied electric field, demonstrating the magnetoelectric coupling. If an out-of-plane electric field is applied, first along the positive x_3 direction, and then switched to negative x_3 direction, then the resulting ferroelastic, ferroelectric, and antiferromagnetic domains before and after the switching are shown in Fig. 7. Again, while the applied electric field is reversed, and 180° domain switching is expected, the evolution path is rather complicated and non-intuitive, and the morphology of final domain configuration after reversal appears to result from a 90° rotation from the original domain configurations before the reversal of electric field. This is consistent with what are observed in experiments using PEEM and piezoresponse force microscopy (Zhao et al., 2006).

7. Concluding remarks

In summary, we have developed an unconventional phase field simulation for multiferroic bismuth ferrite with coupled ferroelastic, ferroelectric, and antiferromagnetic domains, and demonstrated the switching of antiferromagnetic domains of bismuth ferrite by either electric or mechanical loading. Good qualitative agreements with experiments are observed, and the theory offers a powerful tool to study a wide range of magnetoelectric multiferroic materials.

Acknowledgements

We gratefully acknowledge the support of US ARO (W911NF-07-1-0410) and NSF Metal program (DMR-0706100). Shu is also supported by TW NSC (97-2221-E-002-125-MY3).

References

Aharoni, A., 2000. Introduction to the Theory of Ferromagnetism (The International Series of Monographs on Physics). Oxford Science Publications.

Balke, N., Choudhury, S., Jesse, S., Huijben, M., Chu, Y.H., Baddorf, A.P., Chen, L.Q., Ramesh, R., Kalinin, S.V., 2009. Deterministic control of ferroelastic switching in multiferroic materials. Nature Nanotechnology 4, 868–875.

Bhattacharya, K., 1993. Comparison of the geometrically nonlinear and linear theories of martensitic-transformation. Continuum Mechanics and Thermodynamics 5, 205–242.

Bhattacharya, K., James, R., 1999. A theory of thin films of martensitic materials with applications to microactuators. Journal of the Mechanics and Physics of Solids 47, 531–576.

Brown, W.F., 1963. Micromagnetics. Wesley, NY.

Chen, L.Q., 2002. Phase-field models for microstructure evolution. Annual Review of Materials Research 32, 113–140.

Chu, Y.-H., Martin, L.W., Holcomb, M.B., Gajek, M., Han, S.-J., He, Q., Balke, N., Yang, C.-H., Lee, D., Hu, W., Zhan, Q., Yang, P.-L., Fraile-Rodriguez, A., Scholl, A., Wang, S.X., Ramesh, R., 2008. Electric-field control of local ferromagnetism using a magnetoelectric multiferroic. Nature Materials 7, 478–482.

Chung, T.-K., Keller, S., Carman, G.P., 2009a. Electric-field-induced reversible magnetic single-domain evolution in a magnetoelectric thin film. Applied Physics Letters 94, 132501.

Chung, T.-K., Wong, K., Keller, S., Wang, K.L., Carman, G.P., 2009b. Electrical control of magnetic remanent states in a magnetoelectric layered nanostructure. Journal of Applied Physics 106, 103914.

Cruz, M.P., Chu, Y.H., Zhang, J.X., Yang, P.L., Zavaliche, F., He, Q., Shafter, P., Chen, L.Q., Ramesh, R., 2007. Strain control of domain-wall stability in epitaxial $BiFeO_3$(1 1 0) thin films. Physical Review Letters 99, 217601.

Czekaj, S., Nolting, F., Heyderman, L.J., Willmott, P.R., van der Laan, G., 2006. Sign dependence of the X-ray magnetic linear dichroism on the antiferromagnetic spin axis in $LaFeO_3$ thin films. Physical Review B 73, 020401(R).

DeSimone, A., James, R.D., 2002. A constrained theory of magnetoelasticity. Journal of the Mechanics and Physics of Solids 50, 283–320.

Ederer, C., Spaldin, N., 2005a. Effect of epitaxial strain on the spontaneous polarization of thin film ferroelectrics. Physical Review Letters 95, 257601.

Ederer, C., Spaldin, N., 2005b. Influence of strain and oxygen vacancies on the magnetoelectric properties of multiferroic bismuth ferrite. Physical Review B 71, 224103.

Ederer, C., Spaldin, N.A., 2005c. Weak ferromagnetism and magnetoelectric coupling in bismuth ferrite. Physical Review B 71, 060401(R).

Eerenstein, W., Mathur, N.D., Scott, J.F., 2006. Multiferroic and magnetoelectric materials. Nature 442, 759–765.

Eerenstein, W., Morrison, F.D., Dho, J., Blamire, M.G., Scott, J.F., Mathur, N.D., 2005. Comment on "epitaxial $BiFeO_3$ multiferroic thin film heterostructures". Science 307, 1203.

Fiebig, M., 2005. Revival of the magnetoelectric effect. Journal of Physics D 38, R123–R152.

Fiebig, M., Lottermoser, T., Frohlich, D., Goltsev, A.V., Pisarev, R.V., 2002. Observation of coupled magnetic and electric domains. Nature 419, 818–820.

Fischer, P., Polomska, M., Sosnowska, I., Szymanski, M., 1980. Temperature dependence of the crystal and magnetic structure of $BiFeO_3$. Journal of Physics C 13, 1931–1940.

Gilbert, T., 1955. Physical Review 100, 1243.

Hu, H.L., Chen, L.Q., 1998. Three-dimensional computer simulation of ferroelectric domain formation. Journal of the American Ceramic Society 81, 492–500.

Hur, N., Park, S., Sharma, P.A., Ahn, J.S., Guha, S., Cheong, S.W., 2004. Electric polarization reversal and memory in a multiferroic material induced by magnetic fields. Nature 430, 541–544.

Kiselev, S.V., Ozerov, R.P., Zhdanov, G.S., 1963. Detection of magnetic order in ferroelectric $BiFeO_3$ by neutron diffraction. Soviet Physics Doklady 7, 742–744.

Kubel, F., Schimid, H., 1990. Structure of a ferroelectric and ferroelastic monodomain crystal of the perovskite $BiFeO_3$. Acta Crystallographica B 46, 698–702.

Landau, L., Lifshitz, E., 1935. Physik Z Sowjetunion 8, 153.

Landis, C.M., 2008. A continuum thermodynamics formulation for micro-magneto-mechanics with applications to ferromagnetic shape memory alloys. Journal of the Mechanics and Physics of Solids 56, 3059–3076.

Lei, C.H., Li, L.J., Shu, Y.C., Li, J.Y., 2010. Austenite–martensite interface in shape memory alloys. Applied Physics Letters 96, 141910.

Li, J.Y., Liu, D., 2004. On ferroelectric crystals with engineered domain configurations. Journal of the Mechanics and Physics of Solids 52, 1719–1742.

Li, L.J., Li, J.Y., Shu, Y.C., Chen, H.Z., Yen, J.H., 2008a. Magnetoelastic domains and magnetic field-induced strains in ferromagnetic shape memory alloys by phase-field simulation. Applied Physics Letters 92, 172504.

Li, L.J., Li, J.Y., Shu, Y.C., Yen, J.H., 2008b. The magnetoelectric domains and cross-field switching in multiferroic $BiFeO_3$. Applied Physics Letters 93, 192506.

Li, Y.L., Hu, S.Y., Liu, Z.K., Chen, L.Q., 2002. Effect of substrate constraint on the stability and evolution of ferroelectric domain structures in thin films. Acta Materialia 50, 395–411.

Lottermoser, T., 2004. Magnetic phase control by an electric field. Nature 430, 541–544.

Michel, C., Moreau, J.M., Achenbach, G.D., Gerson, R., James, W.J., 1969. The atomic structure of $BiFeO_3$. Solid State Communications 7, 701–704.

Mura, T., 1982. Micromechanics of Defects in Solids. Martinus Nijhoff, Boston.

Nan, C.W., Liu, G., Liu, Y., Chen, H., 2005. Magnetic-field-induced electric polarization in multiferroic nanostructures. Physical Review Letters 94, 197203.

Neaton, J.B., Ederer, C., Waghmare, U.V., Spaldin, N.A., Rabe, K.M., 2005. First-principles study of spontaneous polarization in multiferroic $BiFeO_3$. Physical Review B 71, 014113.

Ramesh, R., Spaldin, N.A., 2007. Multiferroics: progress and prospects in thin films. Nature Materials 6, 21–29.

Ruette, B., Zvyagin, S., Pyatakov, A.P., Bush, A., Li, J.F., Belotelov, V.I., Zvezdin, A.K., Viehland, D., 2004. Magnetic-field-induced phase transition in $BiFeO_3$ observed by high-field electron spin resonance: cycloidal to homogeneous spin order. Physical Review B 69, 064114.

Shu, Y.C., Lin, M.P., Wu, K.C., 2004. Micromagnetic modeling of magnetostrictive materials under intrinsic stress. Mechanics of Materials 36, 975–997.

Shu, Y.C., Yen, J.H., 2007. Pattern formation in martensitic thin films. Applied Physics Letters 91, 021908.

Shu, Y.C., Yen, J.H., 2008. Multivariant model of martensitic microstructure in thin films. Acta Materialia 56, 3969–3981.

Shu, Y.C., Yen, J.H., Chen, H.Z., Li, J.Y., Li, L.J., 2008. Constrained modeling of domain patterns in rhombohedral ferroelectrics. Applied Physics Letters 92, 052909.

Spaldin, N.A., Fiebig, M., 2005. The renaissance of magnetoelectric multiferroics. Science 309, 391–392.

Suess, D., 2002. Micromagnetic simulations of antiferro- and ferromagnetic structures for magnetic recording. Ph.D. Dissertation, Vienna University of Technology.

Teague, J.R., Gerson, R., James, W.J., 1970. Dielectric hysteresis in single crystal $BiFeO_3$. Solid State Communications 8, 1073–1074.

Thole, B.T., van der Laan, G., Sawatzky, G.A., 1985. Strong magnetic dichroism predicted in the m4,5 X-ray absorption spectra of magnetic rare-earth materials. Physical Review Letter 55, 2086–2088.

Tsou, N.T., Huber, J.E., 2010. Compatible domain arrangements and poling ability in oriented ferroelectric films. Continuum Mechanics and Thermodynamics 22, 203–219.

Wang, J., Neaton, J.B., Zheng, H., Nagarajan, V., Ogale, S.B., Liu, B., Viehland, D., Vaithyanathan, V., Schlom, D.G., Waghmare, U.V., Spaldin, N.A., Rabe, K.M., Wuttig, H., Ramesh, R., 2003. Epitaxial $BiFeO_3$ multiferroic thin film heterostructures. Science 299, 1719–1722.

Yang, L., Dayal, K., 2010. Formulation of phase-field energies for microstructure in complex crystal structures. Applied Physics Letters 96, 081916.

Yen, J.H., Shu, Y.C., Shieh, J., Yeh, J.H., 2008. A study of electromechanical switching in ferroelectric single crystals. Journal of the Mechanics and Physics of Solids 56, 2117–2135.

Zavaliche, F., 2005a. Ferroelectric domain structure in epitaxial $BiFeO_3$ films. Applied Physics Letters 87, 182912.

Zavaliche, F., 2005b. Polarization switching in epitaxial $BiFeO_3$ films. Applied Physics Letters 87, 252902.

Zavaliche, F., 2006. Multiferroic $BiFeO_3$ films: domain structure and polarization dynamics. Phase Transitions 79, 991–1017.

Zhang, J.X., Chen, L.Q., 2005. Phase-field model for ferromagnetic shape-memory alloys. Philosophical Magazine Letters 85, 533–541.

Zhang, J.X., Li, Y.L., Choudhury, S., Chen, L.Q., Chu, Y.H., Zavaliche, F., Cruz, M.P., Ramesh, R., Jia, Q.X., 2008. Computer simulation of ferroelectric domain structures in epitaxial $BiFeO_3$ thin films. Journal of Applied Physics 103, 094111.

Zhang, J.X., Li, Y.L., Wang, Y., Liu, Z.K., Chen, L.Q., Chu, Y.H., Zavaliche, F., Ramesh, R., 2007. Effect of substrate-induced strains on the spontaneous polarization of epitaxial $BiFeO_3$ thin films. Journal of Applied Physics 101, 114105.

Zhang, Y.H., Li, J.Y., Fang, D.N., 2010. Size dependent domain configuration and electric field driven evolution in ultrathin ferroelectric films: a phase field investigation. Journal of Applied Physics 107, 034107.

Zhao, T., Scholl, A., Zavaliche, F., Lee, K., Barry, M., Doran, A., Cruz, M.P., Chu, Y.H., Ederer, C., Spaldin, N.A., Das, R.R., Kim, D.M., Baek, S.H., Eom, C.B., Ramesh, R., 2006. Electrical control of antiferromagnetic domains in multiferroic $BiFeO_3$ films at room temperature. Nature Materials 5, 823–829.